The making of natural iron sulfide nanoparticles in a hot vent snail

Satoshi Okada[a,1], Chong Chen[b], Tomo-o Watsuji[c], Manabu Nishizawa[b], Yohey Suzuki[d], Yuji Sano[e,f], Dass Bissessur[g], Shigeru Deguchi[a], and Ken Takai[b]

[a]Research Center for Bioscience and Nanoscience (CeBN), Research Institute for Marine Resources Utilization, Japan Agency for Marine-Earth Science and Technology (JAMSTEC), Yokosuka, 237-0061 Kanagawa, Japan; [b]Institute for Extra-cutting-edge Science and Technology Avant-garde Research (X-star), Japan Agency for Marine-Earth Science and Technology (JAMSTEC), Yokosuka, 237-0061 Kanagawa, Japan; [c]Department of Food and Nutrition, Higashi-Chikushi Junior College, Kitakyusyu, 803-0846 Fukuoka, Japan; [d]Department of Earth and Planetary Science, Graduate School of Science, The University of Tokyo, 113-0033 Tokyo, Japan; [e]Department of Chemical Oceanography, Atmosphere and Ocean Research Institute, The University of Tokyo, Kashiwa, 277-8564 Chiba, Japan; [f]Institute of Surface-Earth System Science, Tianjin University, 300072 Tianjin, P.R. China; and [g]Department for Continental Shelf, Maritime Zones Administration & Exploration, Ministry of Defence and Rodrigues, 11328 Port-Louis, Mauritius

Edited by Lia Addadi, Weizmann Institute of Science, Rehovot, Israel, and approved August 14, 2019 (received for review May 21, 2019)

Biomineralization in animals exclusively features oxygen-based minerals with a single exception of the scaly-foot gastropod *Chrysomallon squamiferum*, the only metazoan with an iron sulfide skeleton. This unique snail inhabits deep-sea hot vents and possesses scales infused with iron sulfide nanoparticles, including pyrite, giving it a characteristic metallic black sheen. Since the scaly-foot is capable of making iron sulfide nanoparticles in its natural habitat at a relatively low temperature (~15 °C) and in a chemically dynamic vent environment, elucidating its biomineralization pathways is expected to have significant industrial applications for the production of metal chalcogenide nanoparticles. Nevertheless, this biomineralization has remained a mystery for decades since the snail's discovery, except that it requires the environment to be rich in iron, with a white population lacking in iron sulfide known from a naturally iron-poor locality. Here, we reveal a biologically controlled mineralization mechanism employed by the scaly-foot snail to achieve this nanoparticle biomineralization, through δ^{34} S measurements and detailed electron-microscopic investigations of both natural scales and scales from the white population artificially incubated in an iron-rich environment. We show that the scaly-foot snail mediates biomineralization in its scales by supplying sulfur through channel-like columns in which reaction with iron ions diffusing inward from the surrounding vent fluid mineralizes iron sulfides.

biomineralization | scaly-foot gastropod | nanoparticle

Many animals produce hard tissues for skeletal support, protection (e.g., turtle shell), and feeding (e.g., molluscan radula), among other purposes. These hard tissues are often mineralized, and well-known examples of the minerals include hydroxyapatite in bones and teeth, calcium carbonate in shells of various invertebrate groups and fish otolith (1), and silica found on hexactinellid sponges (2). These minerals may be either generated by the animals themselves (3) or produced by other organisms such as bacteria before being incorporated by the animals (4). Biominerals found in animals almost always contain oxygen as a common element (i.e., oxides, hydroxides, carbonates, and phosphates), while other group-16 elements such as sulfur, especially as sulfides, are usually not found in minerals in the animal body. Outside eukaryotes, however, sulfur-reducing bacteria are known to convert iron sulfide, FeS (mackinawite), to Fe_3S_4 (greigite) (5, 6).

A rare exception among animals that possess sulfide minerals is a deep-sea snail known as the scaly-foot gastropod (*Chrysomallon squamiferum*) found in hydrothermal vents on the Central Indian Ridge (CIR) in the Indian Ocean (Fig. 1*A*) (7–11). The scaly-foot gastropod is of scientific interest not only because it is the only gastropod that possesses dermal scales on its body (12) but also because it is the only animal that exceptionally possesses sulfide minerals in its body—namely, pyrite (FeS_2) and greigite (Fe_3S_4)—within both its scales and its shell (13). The scale, reported to be proteinaceous and composed chiefly of conchiolin proteins (9, 12), is of special interest because it is often densely infused with iron sulfide nanoparticles (by which we collectively mean pyrite, greigite, and mackinawite hereafter). The level of iron sulfide incorporation varies greatly among different populations inhabiting different vent fields; individuals from the Kairei Field on the CIR (25°19.23′S, 70°02.42′E) possess rich iron sulfide minerals leading to a metallic black coloration (hereafter black scaly-foot) while those from the Solitaire Field (19°33.41′S, 65°50.89′E) on the CIR do not, resulting in a whitish coloration (hereafter white scaly-foot) (Fig. 1*B*) (14). This difference is not due to genetics (15), but appears to be due to the environmental water chemistry where the iron content in the endmember hydrothermal fluid is ~1/58 in the Solitaire Field (60 μM) (16) compared with that in the Kairei Field (3,450 μM) (17). All populations of the scaly-foot snail rely on thioautotrophic endosymbionts living within bacteriocytes inside the snail's "trophosome" (modified esophageal gland), and it has been speculated that the sulfide mineralization may be associated with the need for the snail to circulate hydrogen sulfide within its bloodstream to feed the bacteria (18).

The mechanism of mineralization in the scaly-foot snail, as well as the accumulation pathways of relevant elements, has been debated since its discovery, especially for the nanoparticles seen in its

Significance

Highly adapted to deep-sea hot vents, the scaly-foot gastropod *Chrysomallon squamiferum* is unique among living and extinct animals in possessing an imbricating scale-armor reinforced by iron sulfide nanoparticles. Mechanisms behind its biogenic sulfide synthesis are expected to revolutionize industrial production of metal chalcogenide nanoparticles, but how the gastropod manages such processes remains entirely unknown. Here, using state-of-art microscopy and elemental analyses, we show that the living animal mediates biomineralization of iron sulfide nanoparticles via a channel-like columnar organic matrix that transports sulfur, which then reacts with iron ions diffusing in from the surrounding vent fluid. This allows the snail to make iron sulfide nanoparticles in a dynamic low-temperature environment, opening the potential to significantly reduce the industrial production costs of such particles.

Author contributions: S.O., T.-o.W., S.D., and K.T. designed research; S.O., C.C., T.-o.W., M.N., Y. Suzuki, Y. Sano, and K.T. performed research; S.O., C.C., and M.N. analyzed data; and S.O., C.C., T.-o.W., M.N., Y. Suzuki, Y. Sano, D.B., S.D., and K.T. wrote the paper.

The authors declare no conflict of interest.

This article is a PNAS Direct Submission.

[1]To whom correspondence may be addressed. Email: okadasa@jamstec.go.jp.

This article contains supporting information online at www.pnas.org/lookup/suppl/doi:10.1073/pnas.1908533116/-/DCSupplemental.

First Published September 24, 2019.

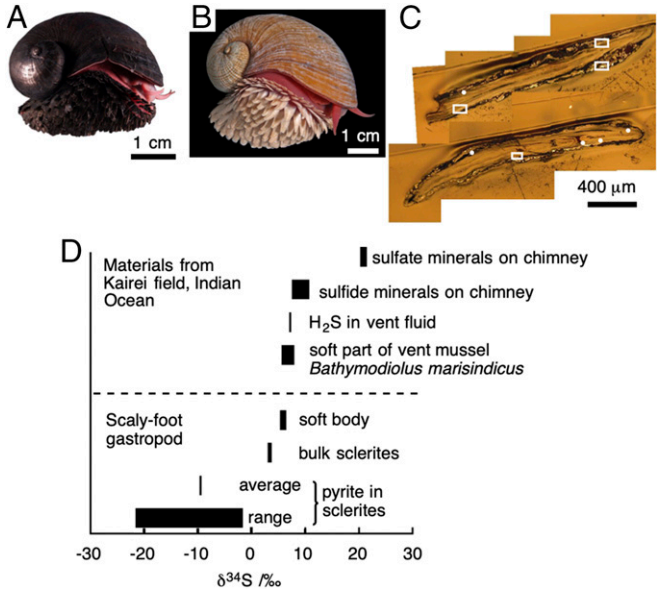

Fig. 1. Nano-SIMS imaging of black scaly-foot scales. (*A*) Black scaly-foot snail. (*B*) White scaly-foot snail. (*C*) Optical micrograph of the cross-section of black scaly-foot scale. White dots and squares are analyzed areas; the detailed data are shown in *SI Appendix*, Fig. S2. (*D*) Summary of $\delta^{34}S$ in comparison with surrounding environments.

scales. Three processes are hypothesized as to how the scaly-foot scales become infused with iron sulfide nanoparticles, including one abiotic process and two biomineralization processes. First, abiotically formed nanoparticles may be incorporated into the scales, as mineral nanoparticles are being produced by the hydrothermal vent itself acting as a high-temperature flow reactor with fluid temperature of 315 °C; these nanoparticles may subsequently find their way into the scales—for example, by being incorporated during secretion (19). Second, sulfur-oxidizing bacteria are abundant around hydrothermal vents and also often occur on the surfaces of animals; such bacteria may biomineralize iron sulfide minerals (5, 10), which subsequently become incorporated into scaly-foot scales. Third, the scaly-foot snail may indeed biomineralize or biologically control the mineralization of iron sulfide nanoparticles by itself, either in the scales or in the secreting epithelium below the scales.

These 3 hypotheses have been suggested but without conclusions due to the lack of information on the source and pathways of iron and sulfur atoms in the scale nanoparticles (13). In the present study, we investigated natural black scaly-foot scales by nanoscale secondary ion mass spectrometry (nanoSIMS) and electron-microscopic analyses, showing evidence that the scaly-foot snail biologically controls the mineralization of iron sulfide nanoparticles. In addition, we show that the scaly-foot snail mediates this unique mineralization process by controlling the accumulation of sulfur through sulfur-enriched, channel-like columnar structures within the scales followed by iron diffusion from seawater, through an in situ experiment where scales removed from the white scaly-foot were incubated in the natural habitat of the black scaly-foot, the Kairei Field.

Results

Isotopic Microanalysis of Native Black Scaly-Foot Scales. Isotopic abundance analyses of ^{32}S and ^{34}S were performed to understand whether the iron sulfide nanoparticles within the scales of the black scaly-foot are products of abiotic production or biomineralization (Fig. 1 *C* and *D*; also see *SI Appendix*, *Methods*, and Fig. S2) (20). NanoSIMS measurements revealed that the sulfur isotope ratio ($\delta^{34}S$) of iron sulfide does not significantly differ between the tip and the base of the scales (around the secreting epithelium), and ranges from –21.6 ± 1.1 to –1.8 ± 0.5‰, with the average being –9.6 ± 0.1‰ (mean ± SD). This value is much lower than that of the environmental sulfur in the CIR, including vent fluids (+6.8 to 7.0‰) (21, 22), sulfide chimneys (+4.4 to 7.5‰) (21), and sulfate minerals (+19.1 to 20.2‰) (22), and also much lower than that of the soft parts of the snail's body (+4.8 ± 0.5‰) (13) and that of the co-occurring deep-sea mussel *Bathymodiolus marisindicus*, which is +3.4‰ for muscle to 5.6‰ for gill (21). It is known that light isotopes are preferentially used in redox metabolisms of bacteria (23, 24), and simple incorporation of abiotic minerals or ions without biological redox reactions essentially does not change the $\delta^{34}S$ from that of naturally occurring minerals. The much lower $\delta^{34}S$ values observed within the scales indicate preferential accumulation of ^{32}S in the scaly-foot snail by certain biological redox functions, implying that they are products of biomineralization.

Microscopic Analyses of Scaly-Foot Scales. Electron-microscopic investigation of the black scaly-foot scale was performed to distinguish the 2 possible biological pathways: biomineralization mediated by microbes or biomineralization by the snail itself. Cross-sectional scanning transmission electron microscopy (STEM) images revealed the existence of 3 layers (Fig. 2*A*; also see *SI Appendix*, Fig. S3), which we distinguished based on the appearance of the particles they contain. The layers were 1) the outermost layer consisting of densely aggregated angular particles (390 ± 196 nm, $n = 173$) up to 6–8 μm; 2) the middle layer consisting of spherical particles (120 ± 91 nm, ranging 26–789 nm, $n = 347$) dispersing up to 19 μm from the surface inward; and 3) the innermost layer containing circular domains (231 ± 78 nm, $n = 152$) with dark-contrasted edges and bright-contrasted center parts. Energy-dispersive X-ray spectroscopy (EDS) analyses confirmed that the dark-contrasted parts are mainly composed of iron sulfide (*SI Appendix*, Fig. S3). The trilayered structure has also been observed under optical microscopy with Richardson's stain (12). The innermost layer has less contrast than the middle layer in both electron and optical micrographs, indicating its lower density. It is important to note that, when viewed macroscopically, this innermost layer represents cumulative growth of the tip of the scale and is exclusively produced by a small portion of the secreting epithelium (12). The differences seen in density, therefore, could be due to differences in the nature of the underlying epithelium or due to the fact that this is a meeting point of 2 "fields" producing the dorsal and ventral sides of the scale (which is very flat) and there may be interference between the 2 fields.

Since the outermost layer is exposed to ambient seawater containing iron sulfide particles originating from the vent fluid and microbes living around the vent orifices, it is highly probable that the iron sulfide minerals in the outermost layer are mainly due to mineral deposition and adsorption onto the body surface of the scaly-foot snail. This is evident from the decreased thickness of the outermost-layer minerals on the scales from the distal tip toward the basal secreting epithelium. As the scales grow incrementally (12), the tips of the scales represent the oldest parts that have had the longest time for minerals to accumulate from the seawater. The scales are also overlapped near the base, scratching each other to partially remove outer mineral deposits (*SI Appendix*, Fig. S4). In addition, rod-shaped iron sulfide minerals with the size of (36 ± 14) × (15 ± 4) nm ($n = 74$) were also observed on the operculum of *Alviniconcha marisindica*, another snail co-occurring with the scaly-foot snail at the Kairei Field (*SI Appendix*, Fig. S5). Interestingly, some of the mineral particles penetrate slightly (~1 μm) into the operculum, but only a single layer of mineral particles could be found predominantly on the outermost surface, which we interpret as abiotically deposited minerals.

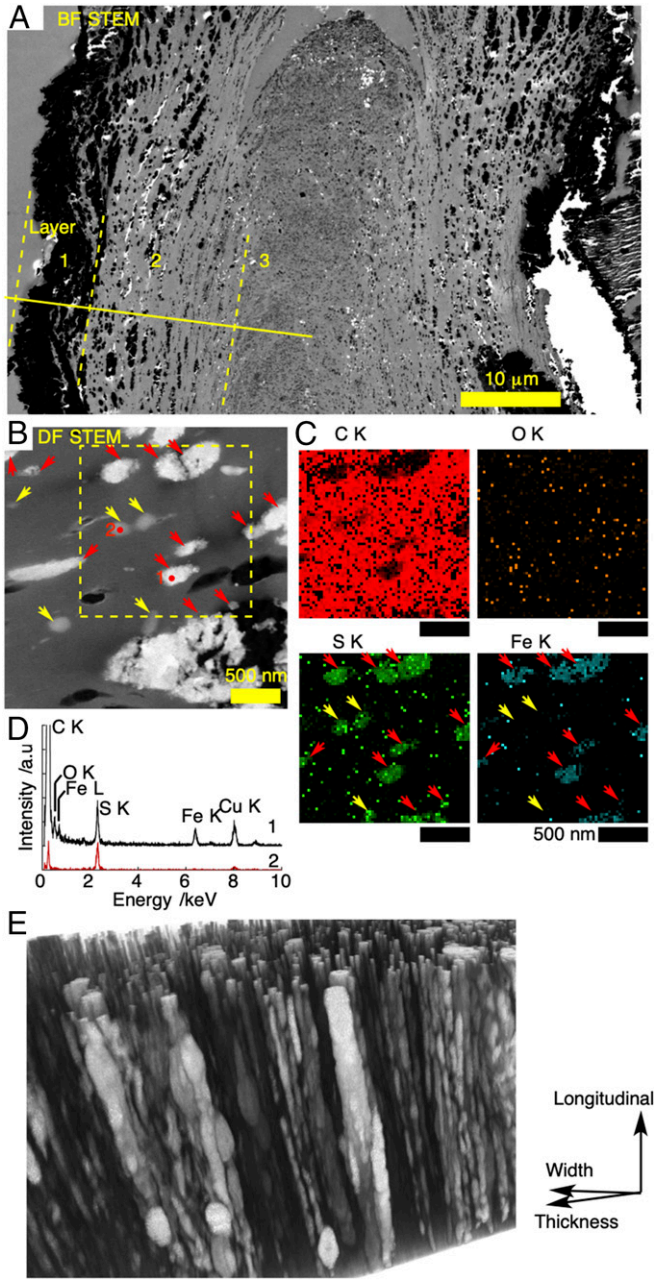

Fig. 2. Electron-microscopic images of black scaly-foot scales. (*A*) Bright-field STEM image of a thin section taken at 25 kV. Boundaries of 3-layered structures are indicated by yellow lines. (*B*) Dark-field STEM image. (*C*) EDS maps of a thin section taken at 120 kV. Red and yellow arrows indicate iron sulfide minerals and sulfur-rich clusters, respectively. (*D*) EDS point analyses of the red dots in *B*: Position 1, mineral clusters; position 2, circular domain rich in sulfur and poor in iron. (*E*) 3D image of a resin-embedded scale showing the channel-like columns.

The middle layer is our major concern, due to the presence of iron sulfide nanoparticles, which a previous publication indicated includes pyrite (13). The particles are aligned along the incremental growth lines that were also visible in an optical micrograph (12). EDS analyses confirmed that the dark-contrasted particles are iron sulfide in all layers (*SI Appendix*, Fig. S3 and Tables S1 and S2). Transmission electron microscopy (TEM) images of the iron sulfide particles in the second layer also showed that the particles are mainly composed of spherical nanoparticles (7.0 ± 3.8 nm, n = 126); nanorods (80 ± 28 nm long, n = 8) were also found as a minor component (*SI Appendix*, Fig. S6). The layered alignment of nanoparticles indicates that nanoparticle growth is correlated with growth of the scales (*SI Appendix*, Fig. S2; also see Fig. 1*B* in ref. 12). The rare nanorods are similar in form and size to the nanorods seen in *Alviniconcha marisindica* operculum and are inferred to have originated from the outside surface. Areas around the mineralized domains are not always filled with tissue and sometimes left as voids.

STEM images of the cross-section of a black scaly-foot scale also revealed the existence of 159 ± 5 nm (n = 7) sulfur-rich domains in the middle layer (Fig. 2 *B*–*D*). STEM-EDS analyses showed that these sulfur-rich domains also contain carbon, nitrogen, and oxygen in quantities similar to those in surrounding tissues, whereas other elements including iron were below the detection limit (*SI Appendix*, Fig. S7). Sizes of the sulfur-rich domains are comparable to those of iron sulfide minerals in the middle layer. These sulfur-rich domains are unique to scaly-foot scales and not observed in other co-occurring vent mollusks, such as *Alviniconcha marisindica* (*SI Appendix*, Fig. S5), which is an indication that the scaly-foot itself enriches sulfur within the scale.

The 3-dimensional (3D) alignment of the minerals was further investigated by focused ion beam (FIB)-SEM followed by 3D reconstruction (*SI Appendix*, Fig. S8 and Movie S1) (25, 26). The image shows that the alignment of mostly mineralized, channel-like columns is along the longitudinal direction of the scale. The contrast of the columns closer to the outer surface was brighter, indicating a gradient of iron concentration perpendicular to the longitudinal direction. The typical diameter of the columns is 100–150 nm, while narrower columns of <50 nm were also found. The mineralized columns are 461 ± 128 nm in distance from each other, which is smaller than that for the typical size of the scale-secreting cells. These morphological features imply that the formation of columns is regulated by the epithelial cells and that several columns are continually constructed from several sites on a single cell. Mineralized granules were also found within the columns which correspond to the circular domains discussed above. These vary in size and form, but are consistently aligned longitudinally along the channel-like columns. Dark-contrasted domains were found within or around the large granules, owing to oxidation during sample storage that caused shrinkage of the crystals (*SI Appendix*, Table S1).

The chemical nature of the black scaly-foot scales was investigated by microscopic transmission infrared spectroscopy from a 1-μm-thick section (*SI Appendix*, Fig. S9). Since the sample thickness was uniform across the thin section, the absorption intensity was directly correlated to the relative amount of corresponding chemical species. Strong absorption bands at 3,122–3,666 and 1,500–1,585 cm^{-1} were found almost uniformly over the scale with similar spacial distribution in intensity. These peaks were assigned to secondary amides in the solid state—namely, *N-H* stretching and bending, respectively. A strong absorption band at 1,585–1,700 cm^{-1} that corresponds to the C = O stretching of amide carbonyl was also distributed across the thin section, indicating that the scale is mostly made of polypeptides or proteins. The intensity of the carbonyl band is higher in the center, indicating the chemical difference in the innermost layer from the outermost and middle layers. The coexisting signal at 1,740 cm^{-1} comes from the carbonyl group of esters, which is included in the epoxy resin.

Pathways of Iron Transport within Scales. The iron atoms that compose sulfide minerals in scaly-foot snail scales may potentially be incorporated from 2 sources: the snail's body tissue or the surrounding seawater. To provide insights into which source the snail utilizes, the interface between the secreting epithelium of the black scaly-foot and the newly formed part of its scale was investigated by STEM/EDS (*SI Appendix*, Fig. S10). EDS maps clearly showed that the newly secreted scale contains sulfur but is free from iron, while

body tissue is poor in sulfur and contains detectable amounts of iron. If the iron atoms in the iron sulfide nanoparticles originate from the snail's body, then iron accumulation around the epithelium as well as within newly formed parts of the scale should have been observed. Therefore, iron atoms do not come from the snail's body and must originate from the surrounding seawater instead. The depletion of sulfur in the scale-secreting tissue and its enrichment in the newly formed part of the scale are suggestive that the sulfur in iron sulfide nanoparticles is provided by the animal and is deposited into the scale as it is formed.

To verify that iron atoms are indeed diffused from the surrounding seawater, a translocation experiment was performed where individual scales removed from dead white scaly-foot specimens were placed in the natural, deepsea black smoker hydrothermal vent habitat of the black scaly-foot (*SI Appendix*, Fig. S11) (27). Since the natural environment of the white scaly-foot is poor in iron ions, the scales are not biomineralized with iron sulfide and do not contain more iron atoms than the detection limit of EDS analyses (*SI Appendix*, Fig. S12). The scales were incubated in situ for 13 d, which is certainly shorter than the life span of the scaly-foot snail because, although the exact life span is unknown, adult scaly-foot snails have been reared alive in aquaria for more than 3 wk (28) and the life span of gastropods is typically more than a year (29). Therefore, any observations from this translocation experiment can be said to have mimicked the processes that take place naturally when the black scaly-foot snail is alive (but without influence from the living animal).

Upon recovery postincubation, the surface of the translocated scale was densely covered with iron sulfide flakes and microbial cells. The flake-like iron sulfide particles were 3–4 μm thick and 480 ± 376 nm long (n = 257), and the microbial cells were 1.67 ± 0.76 μm in length and 0.63 ± 0.18 μm in width (n = 52, Fig. 3*B*). The surface of the microbial cells was covered with platelet crystals containing Fe:S = 1:1 with variable coverage ratios (Fig. 3*C* and *SI Appendix*, Table S3). It should be noted that the nonsymbiotic microbial cells found on the translocated scaly-foot scale (taken from dead white individuals) are not necessarily the same microbe species as epibiotic cells found naturally on living black scaly-foot animals, which likely have specific symbiotic relationships with microbes living on their body surface (10). Thus, the morphology of iron sulfide minerals produced by epibiotic microbes when the snail is alive may differ from the flake-like morphology observed here.

The cross-section of the translocated scale revealed that the iron ions diffused ~6 μm into the scales within 13 d of incubation to form iron sulfide nanoparticles with the size of 176 ± 89 nm (n = 3,626, Fig. 3*A*). High-resolution TEM images of these scales showed that the morphology of iron sulfide minerals within the scales is in the form of aggregated thin nanosheets, unlike those found within natural black scaly-foot scales (*SI Appendix*, Fig. S13). This is possibly attributable to methodological limitations of the translocation experiment, in which the white scaly-foot experienced several thermal cycles, including freezing to –80 °C and thawing, which possibly resulted in denaturation of organic matrices leading to a different mineral morphology. Nevertheless, the presence of newly formed iron sulfide nanoparticles diffusing into the scales during translocation and in situ incubation strongly suggests that the iron within the natural black scaly-foot scales also originates from seawater.

Pathways of Sulfur Enrichment within Scales. Given the results of sulfur isotope analyses indicating a biomineralized source, the only possible path of sulfur incorporation into the scales is from the soft body of the scaly-foot, which is also evident from the SEM-EDS investigation of the secreting interface as described above. The pH of the scaly-foot snail's body fluid supports this path. The pH of the body fluid (from the foot), the blood, and the trophosome-like

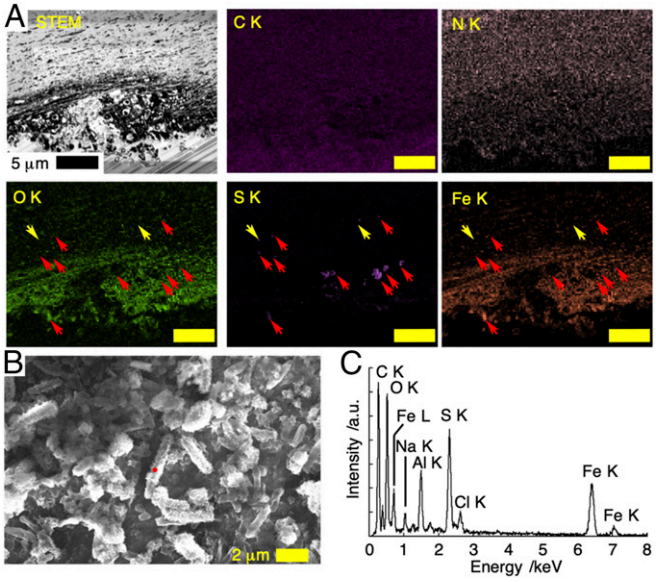

Fig. 3. Cross-section and surface structure of white scaly-foot scale after 13-d incubation in the natural habitat of the black scaly-foot in the Kairei Field, CIR. (*A*) Dark-field STEM image of the thin section with EDS mapping taken at 25 kV; red and yellow arrows indicate sulfur-enriched area with and without iron, respectively. (Scale bars, 5 μm.) (*B*) SEM image of the surface of the translocated scale. (*C*) EDS spectrum of the mineral-coated bacteria indicated by a red dot in *B*.

esophageal gland was averaged among 3 individuals to be 6.83 ± 0.18, 6.76 ± 0.11, and 6.33 ± 0.10 at 21.4 °C and 7.15 ± 0.14, 7.14 ± 0.04, and 6.49 ± 0.09 at 5.2 °C, respectively. These values are considerably lower than the blood pH values of various shallow-water gastropods and bivalves, which generally range between 7.5 and 8.2 (29, 30). Since endosymbionts housed in the scaly-foot snail's trophosome that supply nutrients for the host animal require hydrogen sulfide for their metabolism and energy production (31), it is reasonable to consider the presence of hydrogen sulfide or related species in the blood, which is also supported by the relatively lower pH value in the esophageal gland compared to the blood. The vent-endemic giant tubeworm *Riftia pachyptila*, which has a similar mechanism of housing endosymbionts, is known to take up HS^- instead of H_2S, and the scaly-foot may do the same (32). The calculated first dissociation constant (pK_a) of H_2S being 7.21 based on the water chemistry, along with the temperature of the seawater in the scaly-foot's living environment, also supports HS^- as the plausible species circulating its blood (33). This means that the blood circulation system of the scaly-foot snail can work as a pump to continuously supply hydrogen sulfide to its endosymbionts (18) and to circulate potential sulfur-enriched waste products to be deposited into the scales and removed this way.

Discussion

From the results, we interpret that the scaly-foot snail biologically controls the mineralization of iron sulfide by constructing channel-like sulfur-enriched columns in their scales through which sulfur passes, and allowing a continuous supply of sulfur that then combines with iron ions diffusing in from the seawater. We did not observe any deficit spaces within the columns, indicating that the columns are filled with organic matrices, possibly protein. The scale grows incrementally, layer by layer, from the secreting epithelium (12) along with the scale's organic matrix and the sulfur-enriched columns. The role of the concentrated organic phase is to induce crystallization of minerals as previously observed in collagen-hydroxyapatite systems (34) as well as to regulate the growth of

minerals as utilized in artificial nanoparticle syntheses (35–38). The scaly-foot snail may utilize the sulfur-enriched columns to discard waste sulfur products produced by its endosymbionts, especially considering that the white scaly-foot scales were still rich in sulfur contents (39).

The fact that iron sulfide nanoparticles were present only in the black scaly-foot scale, along with results presented in a previous paper, shows that the mineral species found deep inside the scale is pyrite (FeS_2), and that greigite (Fe_3S_4) is found close to the surface indicates that some form of oxidation is required for mineralization (13). Identification of the iron sulfides discussed here is based on the works of Suzuki et al. (13), and we assume that the small particles in the middle layer are pyrite. The vent fluid is reductive, resulting in the major species of iron and sulfur ions being Fe^{2+} and S^{2-}, whereas the oxidized species of sulfur (i.e., disulfide S_2^{2-}) is required in pyrite and greigite. The potential/pH diagram of the Fe-S-H_2O system shows that the required redox potential is between –0.3 and +0.15 V under physiological conditions (40). Since isotope accumulation is the result of redox reactions, it is assumed that the sulfur species processed or partially oxidized by the symbionts are transported to the foot tissue through the body fluid, and then further transported to the columns of the scales through the secretory epithelium. The sulfur-rich domains found in the columns also indicate the existence of biogenic activity that fixes sulfides within the scales.

Based on our observations, the mechanism of the scaly-foot snail's biologically controlled iron sulfide mineralization within the scales is summarized in Fig. 4. During the secretion of scales by the underlying epithelium, sulfur-diffusive channel-like columns are constructed and then filled with an organic matrix so that sulfur ion diffusion is facilitated. The scale grows by adding layers largely comprising organic matrices, and the sulfur ions as well as the unknown oxidant from the scaly-foot's body fluid circulation diffuse toward the columns. Iron ions diffuse inward from the outside surface of the scale and react with the sulfur ions in the columns to form iron sulfide. The crystal growth of the iron sulfide minerals is regulated by the organic matrices of the columns to produce nanoparticles, and the size of the nanoparticle aggregate is primarily limited by the diameter of the column. The coexisting oxidants possibly lead to chemical transformation of iron sulfide minerals as well as sulfide ions, which are then trapped on the wall of the channel to form sulfur-enriched domains. Since the concentration of iron ions increases around the surface while other conditions remain the same, an iron-rich mineral species [i.e., greigite (Fe_3S_4)] is prone to be formed close to the surface of the scale, leading to the 3 different chemical species of iron sulfide as previously observed (13). The concentration gradient of the iron ions also explains the size difference of the iron sulfide minerals observed between the 3 layers of the scale (Fig. 2*A*).

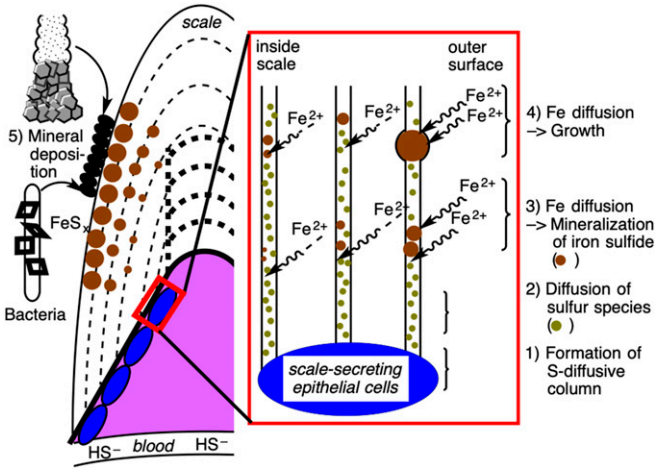

Fig. 4. Schematics of plausible mechanisms of iron sulfide mineralization in the scaly-foot snail. Scale-secreting epithelial cells produce sulfur-enriched channel-like columns (*1*) in which sulfur species are spontaneously diffused outward to the scale (*2*). Iron ions diffuse from the surrounding seawater and react with the sulfur species within the column to mineralize iron sulfides (*3*) and further grows depending on the iron concentration (i.e., distance from the surface) (*4*). Minerals generated in the surrounding environment are also deposited on the scales to form the outermost layer (*5*).

The biomineralization of unusual materials in deep-sea organisms provides key insights for low-energy fabrication of functional materials [e.g., optical fiber in the hexactinellid sponge *Euplectella aspergillum* (2)]. Pyrite, being an earth-abundant and nontoxic semiconducting material, also requires high temperatures, typically over 180 °C, for conventional artificial production using either chemical vapor deposition (41) or hydrothermal synthesis (23, 42). Pyrite is considered to have a wide range of industrial applications in solar cells (43, 44), lithium batteries (42), photodetectors (45), thermoelectric materials (46), and water-splitting catalysts (47). The low-cost manufacturing of pyrite nanoparticles is much desired for facilitating research toward their industrial application. Since simple mixing of Fe^{2+} and H_2S results in formation of FeS and not FeS_2, there is a possibility that deep-sea biological environments such as pressure and the setting within an organic matrix are the key requirements for the formation of pyrite and greigite mineral species. The biologically controlled mechanisms for pyrite production elucidated here are applicable at low temperatures and in a dynamic environment. Although the process is mediated by the scaly-foot snail itself, our translocation experiment exemplifies that the formation of iron sulfide nanomaterials through this mechanism does not require the involvement of a living animal, as long as the chemical and physical framework (i.e., scales infused with sulfur-rich domains) is present. This serves to significantly raise the practicality of adopting it in future industrial processes that are not limited to iron nanoparticles. Of course, much still remains to be learned about the detailed chemistry of the organic matrices involved, including the specific chemical species and kinetics of reduction, the genomic mechanisms involved in synthesis of these organic materials (likely protein), and the mechanisms behind the accumulation of organic material in the sulfur-rich domains. Nevertheless, this biomineralization pathway opens the potential to significantly reduce the industrial production costs of such particles.

Methods

Animal Samples. Black scaly-foot individuals were collected using a slurp-gun during manned submersible DSV *Shinkai 6500* dive #662, February 20, 2001, on R/V *Yokosuka* cruise YK01-15, and during dive #1330, March 16, 2013, on R/V *Yokosuka* cruise YK13-03. They were dehydrated in 99% ethanol. White scaly-foot specimens were collected during DSV *Shinkai 6500* dives #1326, February10, 2013, and #1327, February 11, 2013, on R/V *Yokosuka* cruise YK13-02. They were immediately frozen at –80 °C upon recovery. *Alvinoconcha marisindica* was collected using a slurp-gun during DSV *Shinkai 6500* dive #1458, February 27, 2016, on R/V *Yokosuka* cruise YK16-E02. They were frozen at –80 °C upon recovery.

In Situ Translocation of White Scaly-Foot Samples. Scales for artificial translocation were dissected from the frozen white scaly-foot samples as described above. Six pieces of scale from a thawed white scaly-foot were wrapped in a polyester net, placed in a stainless steel cage (18 × 13 × 8 cm, 10 × 37-mm mesh), and deployed in the natural habitat of the black scaly-foot in the mixing zone between diffusing hydrothermal fluid and seawater in the Kairei Field, CIR, during DSV *Shinkai 6500* dive #1450, February 14, 2016 (25°19.2263′S, 70°2.4190′E, D = 2,424 m; Fig. 1) on R/V *Yokosuka* cruise YK16-E02. After 13 d of incubation, the samples were recovered during DSV *Shinkai 6500* dive #1458, February 27, 2016, on the same cruise. They were frozen at –80 °C upon recovery.

ACKNOWLEDGMENTS. The authors thank the captain and crew of R/V *Yokosuka* as well as the pilots and the technical team of DSV *Shinkai 6500*

during expeditions YK13-02 (cruise principal investigator: Manabu Nishizawa), YK13-03 (cruise principal investigator: Kentaro Nakamura), and YK16-E02 (cruise principal investigator: Ken Takai) for their great support of this scientific activity. All scientists on the expeditions are gratefully acknowledged for their tireless work. Katsuyuki Uematsu (Marine Works Japan Ltd.) is gratefully acknowledged for providing advice and support during electron microscopy. Suguru Nemoto (Enoshima Aquarium) is thanked for providing photos of live scaly-foot snails. We thank the anonymous reviewers, especially reviewer 1, for their critical suggestions, which greatly improved our paper. This study was supported by Japan Society for the Promotion of Science (JSPS) KAKENHI Grants JP16H07490 (to S.O.), JP22540499 (to M.N.), and JP26287133 (to Y. Suzuki).

1. Q. Feng, Principles of calcium-based biomineralization. *Prog. Mol. Subcell. Biol.* **52**, 141–197 (2011).
2. J. Aizenberg, V. C. Sundar, A. D. Yablon, J. C. Weaver, G. Chen, Biological glass fibers: Correlation between optical and structural properties. *Proc. Natl. Acad. Sci. U.S.A.* **101**, 3358–3363 (2004).
3. J. W. Morse, R. S. Arvidson, A. Lüttge, Calcium carbonate formation and dissolution. *Chem. Rev.* **107**, 342–381 (2007).
4. N. K. Dhami, M. S. Reddy, A. Mukherjee, Biomineralization of calcium carbonates and their engineered applications: A review. *Front. Microbiol.* **4**, 314 (2013).
5. M. Pósfai, P. R. Buseck, D. A. Bazylinski, R. B. Frankel, Iron sulfides from magnetotactic bacteria: Structure, composition, and phase transitions. *Am. Mineral.* **83**, 1469–1481 (1998).
6. S. Lin, F. Krause, G. Voordouw, Transformation of iron sulfide to greigite by nitrite produced by oil field bacteria. *Appl. Microbiol. Biotechnol.* **83**, 369–376 (2009).
7. J. Hashimoto, S. Ohta, T. Gamo, H. Chiba, T. Yamaguchi, First hydrothermal vent communities from the Indian Ocean discovered. *Zool. Sci.* **18**, 717–721 (2001).
8. C. L. Van Dover *et al*., Biogeography and ecological setting of Indian Ocean hydrothermal vents. *Science* **294**, 818–823 (2001).
9. A. Warén, S. Bengtson, S. K. Goffredi, C. L. Van Dover, A hot-vent gastropod with iron sulfide dermal sclerites. *Science* **302**, 1007 (2003).
10. S. K. Goffredi, A. Warén, V. J. Orphan, C. L. Van Dover, R. C. Vrijenhoek, Novel forms of structural integration between microbes and a hydrothermal vent gastropod from the Indian Ocean. *Appl. Environ. Microbiol.* **70**, 3082–3090 (2004).
11. C. Chen, K. Linse, J. T. Copley, A. D. Rogers, The "scaly-foot gastropod": A new genus and species of hydrothermal vent-endemic gastropod (Neomphalina: Peltospiridae) from the Indian Ocean. *J. Molluscan Stud.* **81**, 322–334 (2015).
12. C. Chen, J. T. Copley, K. Linse, A. D. Rogers, J. Sigwart, How the mollusc got its scales: Convergent evolution of the molluscan scleritome. *Biol. J. Linn. Soc. Lond.* **114**, 949–954 (2015).
13. Y. Suzuki *et al*., Sclerite formation in the hydrothermal-vent "scaly-foot" gastropod—Possible control of iron sulfide biomineralization by the animal. *Earth Planet. Sci. Lett.* **242**, 39–50 (2006).
14. K. Nakamura *et al*., Discovery of new hydrothermal activity and chemosynthetic fauna on the Central Indian Ridge at 18°–20° S. *PLoS One* **7**, e32965 (2012).
15. C. Chen, J. T. Copley, K. Linse, A. D. Rogers, Low connectivity between "scaly-foot gastropod" (Mollusca: Peltospiridae) populations at hydrothermal vents on the Southwest Indian Ridge and the Central Indian Ridge. *Org. Divers. Evol.* **15**, 663–670 (2015).
16. S. Kawagucci *et al*., Fluid chemistry in the Solitaire and Dodo hydrothermal fields of the Central Indian Ridge. *Geofluids* **16**, 988–1005 (2016).
17. R. M. Gallant, K. L. Von Damm, Geochemical controls on hydrothermal fluids from the Kairei and Edmond vent fields, 23°–25° S, Central Indian Ridge. *Geochem. Geophys. Geosyst.* **7**, Q06018 (2006).
18. C. Chen, K. Uematsu, K. Linse, J. D. Sigwart, By more ways than one: Rapid convergence at hydrothermal vents shown by 3D anatomical reconstruction of Gigantopelta (Mollusca: Neomphalina). *BMC Evol. Biol.* **17**, 62 (2017).
19. M. Yücel, A. Gartman, C. S. Chan, G. W. Luther, Hydrothermal vents as a kinetically stable source of iron-sulphide-bearing nanoparticles to the ocean. *Nat. Geosci.* **4**, 367–371 (2011).
20. M. Nishizawa, S. Maruyama, T. Urabe, N. Takahata, Y. Sano, Micro-scale (1.5 μm) sulphur isotope analysis of contemporary and early Archean pyrite. *Rapid Commun. Mass Spectrom.* **24**, 1397–1404 (2010).
21. T. Yamanaka *et al*., Sulphur-isotopic composition of the deep-sea mussel *Bathymodiolus marisindicus* from currently active hydrothermal vents in the Indian Ocean. *J. Mar. Biol. Assoc. U. K.* **83**, 841–848 (2003).
22. T. Gamo *et al*., Chemical characteristics of newly discovered black smoker fluids and associated hydrothermal plumes at the Rodriguez Triple Junction, Central Indian Ridge. *Earth Planet. Sci. Lett.* **193**, 371–379 (2001).
23. A. Akhoondi, M. Aghaziarati, N. Khandan, Production of highly pure iron disulfide nanoparticles using hydrothermal synthesis method. *Appl. Nanosci.* **3**, 417–422 (2013).
24. D. Canfield, Biogeochemistry of sulfur isotopes. *Rev. Mineral. Geochem.* **43**, 607–636 (2001).
25. C. S. Xu *et al*., Enhanced FIB-SEM systems for large-volume 3D imaging. *Elife* **6**, e25916 (2017).
26. K. Narayan, S. Subramaniam, Focused ion beams in biology. *Nat. Methods* **12**, 1021–1031 (2015).
27. K. Takai *et al*., "R/V Yokosuka & DSV Shinkai 6500 cruise report YK16-E02: geochemical, geomicrobiological and biogeographical investigation of deep-sea hydrothermal activities in the Central and Southwestern Indian Ridges" in *YOKOSUKA YK16-E02 Cruise Data*. https://doi.org/10.17596/0001681. Accessed 29 March 2019.
28. M. Kitada, M. Hiroshi, Y. Suzuki, K. Takai, (2007) On collection and onboard breeding of vent livings collected in Kairei field, Indian Ocean including *Crysomallon squamiferum*. (Yokohama).
29. V. T. Dang, K. Benkendorff, T. Green, P. Speck, S. P. Goff, Marine snails and slugs: A great place to look for antiviral drugs. *J. Virol.* **89**, 8114–8118 (2015).
30. O. Brix, "Blood respiratory properties in marine gastropods" in *The Mollusca*, P. W. Hochachka, Ed. (Academic Press, New York, 1983), pp. 51–75.
31. C. Chen, J. T. Copley, K. Linse, A. D. Rogers, J. D. Sigwart, The heart of a dragon: 3D anatomical reconstruction of the "scaly-foot gastropod" (Mollusca: Gastropoda: Neomphalina) reveals its extraordinary circulatory system. *Front. Zool.* **12**, 13 (2015).
32. S. K. Goffredi, J. J. Childress, N. T. Desaulniers, F. J. Lallier, Sulfide acquisition by the vent worm *Riftia pachyptila* appears to be via uptake of HS-, rather than H2S. *J. Exp. Biol.* **200**, 2609–2616 (1997).
33. M. B. Goldhaber, I. R. Kaplan, Apparent dissociation constants of hydrogen sulfide in chloride solutions. *Mar. Chem.* **3**, 83–104 (1975).
34. Y. Wang *et al*., The predominant role of collagen in the nucleation, growth, structure and orientation of bone apatite. *Nat. Mater.* **11**, 724–733 (2012).
35. Y. M. A. Yamada, T. Arakawa, H. Hocke, Y. Uozumi, A nanoplatinum catalyst for aerobic oxidation of alcohols in water. *Angew. Chem. Int. Ed. Engl.* **46**, 704–706 (2007).
36. M. Nemanashi, J.-H. Noh, R. Meijboom, Dendrimers as alternative templates and pore-directing agents for the synthesis of micro- and mesoporous materials. *J. Mater. Sci.* **53**, 12663–12678 (2018).
37. A. Ethirajan, K. Landfester, Functional hybrid materials with polymer nanoparticles as templates. *Chemistry* **16**, 9398–9412 (2010).
38. K. P. Divya *et al*., In situ synthesis of metal nanoparticle embedded hybrid soft nanomaterials. *Acc. Chem. Res.* **49**, 1671–1680 (2016).
39. C. K. Carney, S. R. Harry, S. L. Sewell, D. W. Wright, "Detoxification biominerals" in *Biomineralization I*, K. Naka, Ed. (Springer, Berlin, 2007), pp. 155–185.
40. D. Kocabag, H. L. Shergold, G. H. Kelsall, Natural oleophilicity/hydrophobicity of sulphide minerals, II. Pyrite. *Int. J. Miner. Process.* **29**, 211–219 (1990).
41. L. Samad *et al*., Direct chemical vapor deposition synthesis of phase-pure iron pyrite (FeS_2) thin films. *Chem. Mater.* **27**, 3108–3114 (2015).
42. J. Liu *et al*., Carbon-encapsulated pyrite as stable and earth-abundant high energy cathode material for rechargeable lithium batteries. *Adv. Mater.* **26**, 6025–6030 (2014).
43. A. Ennaoui, H. Tributsch, Iron sulphide solar cells. *Sol. Cells* **13**, 197–200 (1984).
44. A. Kirkeminde *et al*., Synthesis and optoelectronic properties of two-dimensional FeS_2 nanoplates. *ACS Appl. Mater. Interfaces* **4**, 1174–1177 (2012).
45. M. Gong *et al*., Iron pyrite (FeS_2) broad spectral and magnetically responsive photodetectors. *Adv. Opt. Mater.* **1**, 78–83 (2013).
46. C. Uhlig *et al*., Nanoscale FeS_2 (pyrite) as a sustainable thermoelectric material. *J. Electron. Mater.* **43**, 2362–2370 (2014).
47. B. C. M. Martindale, E. Reisner, Bi-functional iron-only electrodes for efficient water splitting with enhanced stability through in situ electrochemical regeneration. *Adv. Energy Mater.* **6**, 1502095 (2016).